



Effect of Prior Cold Deformation on the Stability of Retained Austenite in GCr15 Bearing Steel

Feng Wang^{1,2} · Dong-Sheng Qian^{1,2} · Xiao-Hui Lu^{2,3}

Received: 29 April 2018 / Revised: 5 June 2018 / Published online: 3 August 2018
© The Chinese Society for Metals and Springer-Verlag GmbH Germany, part of Springer Nature 2018

Abstract

In this work, the effect of prior cold deformation on the stability of retained austenite in GCr15 bearing steel was investigated after quenching and tempering treatment. The thermal stability was evaluated by calculating thermal activation energy for decomposition of retained austenite using differential scanning calorimeter. The mechanical stability was investigated according to the strain-induced martensitic transformation behavior of retained austenite under the standard compression testing. It is found that the prior cold deformation not only accelerates the carbide dissolution during the austenitization process but also contributes to the carbon partitioning in the tempering stage due to the higher density of phase boundaries, which results in the improvement of the thermal stability of retained austenite. Due to the enhanced carbide dissolution, the higher carbon content in the prior austenite will intensify the isotropic strain of martensitic transformation. As a consequence, the film-like retained austenite is likely to form under a higher hydrostatic pressure and thus shows a higher mechanical stability. Additionally, it is noteworthy that the benefits of the prior cold deformation to the stability of retained austenite would be saturated when the cold deformation degree is larger than 40%.

Keywords GCr15 bearing steel · Prior cold deformation · Retained austenite stability

1 Introduction

GCr15 bearing steel, with high carbon and chromium concentrations, is most widely used for bearings. It is routinely treated by spheroidizing, quenching and tempering (QT) to obtain a microstructure comprised of spherical carbides, small amount of retained austenite and tempered martensite. Generally, with the goal of the ring-forming for bearings, GCr15 bearing steel needs to be subjected to cold deformation prior to QT heat treatment [1]. It has been

reported that the prior cold deformation would facilitate the dissolution of carbides by accelerating the austenite transformation [2]. Thus, it can be expected that the carbon content in the martensite matrix would increase with the prior cold deformation, which is in favor of enhancing the hardness but unfavorable for the impact toughness. However, due to the effect of refined prior austenite grain size, the moderate cold deformation (30%) combined with QT process would still increase the impact toughness [3]. In addition, when the imposition of cold deformation is up to 50%, the microcracks may be created at the interfaces between the large carbide particles and the matrix, which is detrimental to the final fatigue performance of bearing steel [4]. Therefore, these researches have shown that the prior cold deformation plays a crucial role in determining the microstructure evolution and mechanical property after QT heat treatment.

Retained austenite is a metastable phase at room temperature and would transform to martensite when sufficient thermal or mechanical activation energy is given. The stability of retained austenite is a key factor to determine the maintenance of accuracy for the engineering application of bearing [5]. In this aspect, the researchers have

Available online at <http://link.springer.com/journal/40195>

✉ Dong-Sheng Qian
qiands@whut.edu.cn

✉ Xiao-Hui Lu
xhlu@whut.edu.cn

¹ School of Materials Science and Engineering, Wuhan University of Technology, Wuhan 430070, China

² Hubei Key Laboratory of Advanced Technology for Automotive Components, Wuhan 430070, China

³ School of Automotive Engineering, Wuhan University of Technology, Wuhan 430070, China

made great efforts to investigate the influencing factors on the stability of retained austenite. Several works showed that the carbon content of retained austenite was responsible for its thermal stability [6, 7], whereas the grain size and morphology of retained austenite determined its mechanical stability [8, 9]. By understanding the factors contributing to mechanical and thermal stabilities of retained austenite, researchers focused on the influence of heat treatment process on retained austenite for the design and processing of bearing steel. For instance, a lower austenitization temperature results in a finer martensitic structure and a higher decomposition activation energy for retained austenite [10]. A slower quenching rate could decrease the potential for martensite nucleation by facilitating the diffusion of carbon atoms to defects [11], which would stabilize the retained austenite effectively. In addition, the cryogenic treatment, as a supplemental process of traditional QT heat treatment, is in favor of the carbon partitioning during the subsequent tempering process [12], thus leading to an increase in the carbon content and thermal stability of retained austenite.

Although the influencing factors on the stability of retained austenite have been extensively studied under different heat treatment parameters, there are few systematic researches focusing on the effect of prior cold deformation on the microstructure and the stability of retained austenite after QT treatment. The aim of the current study is therefore to investigate the relationship between prior cold deformation and stability of retained austenite. In addition, the carbide dissolution and carbon partitioning behaviors during the QT treatment were also discussed.

2 Experimental

2.1 Specimen Preparation

The chemical composition of the steel used in this study is presented in Table 1. The investigated material was received as spheroidize-annealed bar with a diameter of 60 mm and an initial microstructure of spherical carbides in ferritic matrix. The initial volume fraction and diameter of carbides determined by optical image analysis were 12.7% and 0.53 μm , respectively. Standard compression testing was performed at a displacement rate of 1 mm/min at ambient temperature using a SHT4106 universal testing

machine. Specimens for prior cold deformation were cut into a size of ϕ 8 mm \times 20 mm by wire electrode and different cold deformation degrees (0, 10, 20, 30, 40 and 50%) were applied. It is noted that 0% represents the non-deformed specimen in this work. After compression testing, the specimens were austenitized at 860 $^{\circ}\text{C}$ for 30 min under a vacuum condition. Then, the specimens were quenched into oil (60 $^{\circ}\text{C}$) and finally tempered at 160 $^{\circ}\text{C}$ for 2 h.

2.2 Microstructure Observations

A Bähr DIL 805A dilatometer was used to determine the M_S temperature of the non-deformed and deformed specimens with a size of ϕ 4 mm \times 10 mm based on the tangent method [13]. The prepared dilatometry specimens were heated up to a temperature of 860 $^{\circ}\text{C}$, followed by an isothermal holding for 30 min, and then cooled down to ambient temperature at a cooling rate of 30 $^{\circ}\text{C}/\text{s}$. In addition, X-ray diffraction (XRD) data were recorded on a Rigaku D/MAX-RB diffraction analyzer at 12 kW and the tests for each condition were repeated three times to obtain the error bars. The volume fraction of retained austenite was evaluated by the following equations [14]:

$$V_{\alpha} + V_{\gamma} = 1, \quad (1)$$

$$V_{\gamma} = (1.4I_{\gamma}) / (I_{\alpha} + 1.4I_{\gamma}), \quad (2)$$

where V_{α} and V_{γ} represent volume fractions of martensite and austenite, respectively; I_{γ} represents the average of diffraction peak intensities of 220 $_{\gamma}$ and 311 $_{\gamma}$; and I_{α} represents the diffraction peak intensity of 211 $_{\alpha}$.

The carbon concentration in retained austenite was calculated by using lattice parameters obtained from 220 $_{\gamma}$ peak, as expressed by Eq. (3) [15]:

$$a_{\gamma} = 3.5467 + 0.0467C_{\gamma}. \quad (3)$$

The microstructure of QT-treated specimens was examined by a field emission scanning electron microscope (FESEM, FEI Quanta 450) equipped with an electron back-scattered diffraction (EBSD) detector. The specimens for SEM were etched in an alcohol solution containing 4% nitric acid (volume fraction) for 10 s to investigate the microstructure and carbide dissolution behavior. The specimens for EBSD were vibratory polished with colloidal silica after the mechanical finish of 0.5 μm . Meanwhile, Image-pro Plus and Photoshop software were utilized to analyze the size and morphology of the undissolved carbides. The total number of carbide particles measured in the micrographs ranged from 1229 to 1582, and the error bars were determined from the standard deviation of the mean statistical results. To distinguish the prior austenite grain boundaries, the specimens were etched at 65 $^{\circ}\text{C}$ for

Table 1 Chemical compositions of GCr15 bearing steel (wt%)

C	Cr	Si	Mn	Al	P	Fe
0.97	1.56	0.35	0.41	0.07	0.006	Bal.

30 s with a solution consisting of saturated picric acid and small amount of Teepol wetting agent. Optical microscopy (Carl Zeiss, AXIO, A1) was employed to obtain the micrographs for measuring the prior austenite grain size based on linear intercept method. The prior austenite grain size was analyzed according to six fields distributed in different regions, and at least 300 grains were measured in each condition. In order to observe the morphology of retained austenite, transmission electron microscopy (TEM) experiments were carried out on a JEOL 2100F transmission electron microscope operating at 200 kV. The specimens for TEM were prepared by mechanically polishing and then electro-polishing in a twin-jet polisher using a solution of 10% perchloric acid and 90% acetic acid. Besides, the Vickers hardness of QT-treated specimens was measured by using the HV-1000A Vickers hardness tester and each error bar represents the standard deviation of six indents.

2.3 Stability of Retained Austenite

2.3.1 Characterization of Thermal Stability

Differential scanning calorimetry (DSC) was performed using a PerkinElmer Pyris 1 calorimeter to determine the activation energy for the decomposition of retained austenite. The specimens were cut into ϕ 4 mm \times 0.5 mm and then heated from ambient temperature to 400 °C at different heating rates of 5, 10, 15, 20 °C/min, respectively. To ensure the reproducibility of the data, the DSC tests at every heating rate were repeated three times and error bars present the standard deviation. The activation energy was calculated by using the Kissinger equation based on the peak temperature at different heating rates, as expressed by Eq. (4) [16]:

$$\ln(T_p^2/\dot{\theta}) = E/(RT_p) + A, \quad (4)$$

where T_p represents the peak temperature of the transformation at each heating rate; R represents the universal gas constant (8.314 J/mol/K); $\dot{\theta}$ represents the heating rate and A is a constant. The activation energy (E) for the decomposition of retained austenite was obtained through the calculated slope between $\ln(T_p^2 \cdot \dot{\theta}^{-1})$ and $(RT_p)^{-1}$.

2.3.2 Characterization of Mechanical Stability

To investigate the strain-induced martensitic transformation of retained austenite, the compressive strain (10%) with a rate of 1 mm/min was performed using SHT4106 universal testing machine. Each sample (after QT treatment) was cut into a column with a size of ϕ 6 mm \times 9 mm by wire electrode. The volume fraction of retained

austenite before and after compressive strain was measured by XRD. Then, the mechanical stability can be evaluated by the exponential decay law as used by Sugimoto et al. [17]

$$f_{RA_\varepsilon} = f_{RA_0} \cdot \exp(-k\varepsilon), \quad (5)$$

where ε represents the true strain of compression, and f_{RA_0} and f_{RA_ε} represent the volume fraction of retained austenite without strain and at a compressive strain (ε), respectively. k is a constant which reflects the transition degree of retained austenite where a lower k corresponds to a higher mechanical stability of the retained austenite.

3 Results and Discussion

3.1 Microstructure

Figure 1 shows the prior austenite grain boundaries of the QT-treated specimens with cold deformation degree of 0, 20 and 50%. The prior austenite grain size was apparently refined after subjecting to prior cold deformation, which is attributed to the increasing nucleation sites (dislocation and sub-grain) supplied by the prior cold deformation during the ferrite to austenite transformation. From the statistical results in Fig. 2, the prior austenite grain sizes are 9.2, 5.5 and 5.4 μ m at the deformation degree with 0, 40 and 50%, indicating that the refinement of prior austenite grain tends to be saturated when the cold deformation degree reaches 40%. The reason is that the nucleation sites introduced by cold deformation may be saturated after a certain degree of deformation.

The SEM micrographs of the QT-treated specimens are presented in Fig. 3, which shows the microstructures consisting of undissolved spherical carbides (SC), tempered martensite (TM) and small amount of retained austenite (RA). For quantitative analysis, the variation of volume fraction of carbides with different deformation degree was further measured. The volume fraction of undissolved carbides (Fig. 4a) decreases from 7.4 to 5.1% with increasing cold deformation from 0 to 50%. In addition, the average diameter and the aspect ratio of carbide particles were measured, as shown in Fig. 4b. With increasing cold deformation from 0 to 50%, the average diameter of undissolved carbides decreases from 0.72 to 0.54 μ m, and the aspect ratio of carbides increases from 0.71 to 0.79. Thus, it can be concluded that the cold deformation not only facilitates the carbide dissolution but also refines the carbides and improves their roundness.

Under an identical heat treatment parameter, the variation of the carbide dissolution should be ascribed to the difference in the initial microstructure influenced by prior cold deformation. Speich and Szirmae [18] have shown

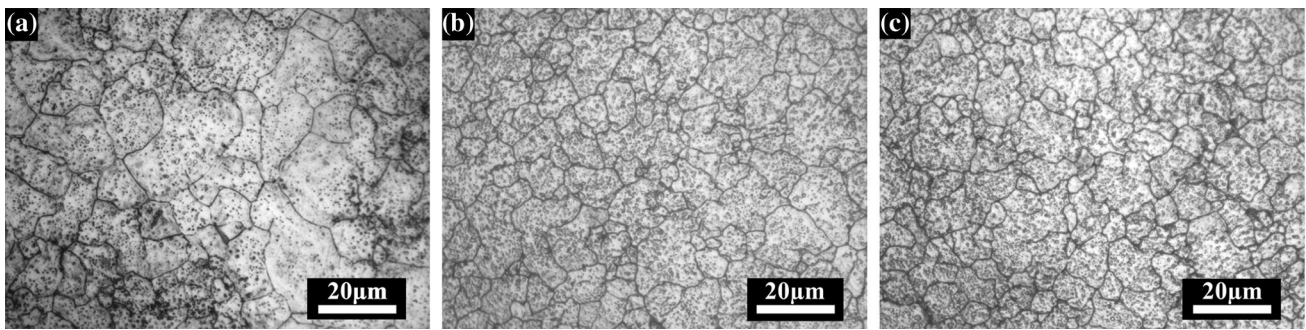


Fig. 1 Prior austenite grain boundaries of the QT-treated specimens with different deformation degrees: a 0%; b 20%; c 50%

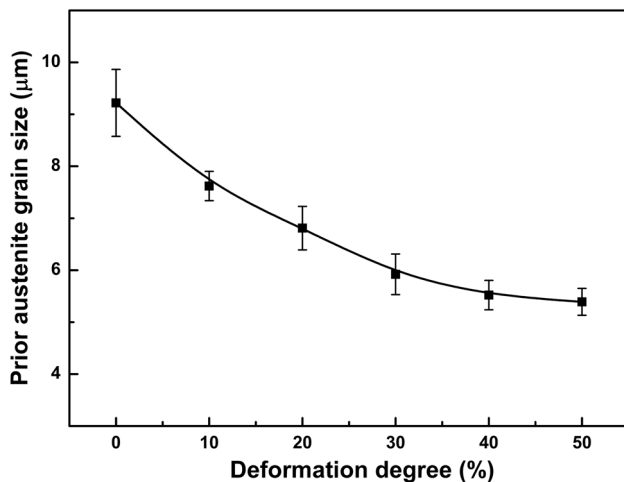


Fig. 2 Average prior austenite grain size of the QT-treated specimens

that austenite is preferentially nucleated at the junction of carbides and ferrite grain boundaries during austenitization. For the spheroidized microstructure subjected to cold deformation, the surface-to-volume ratio between carbides and matrix will increase due to the fragmentation of carbides [19]. Also, fine sub-grains microstructures can be observed for the cold-worked bearing steel [2]. Thus, it can be assumed that more favored nucleation sites are supplied due to the increased interface between carbides and ferrite grain, thereby accelerating the transformation of ferrite to austenite during the austenitization process. Consequently,

the carbide dissolution was accelerated with the increase in cold deformation degree.

Examples of dilatometry curves for the cooling process are shown in Fig. 5a, which indicates that the prior cold deformation with a degree of 50% leads to a decrease in the M_S temperature from 222 to 205 °C. Meanwhile, the retained austenite content with respect to different cold deformation degree was determined via XRD spectrums (Fig. 5b), and the results are shown in Fig. 5c. It is found that retained austenite content after QT treatment increases from 13.7 to 16.8% with increasing deformation from 0 to 50%, which may be attributed to the carbon enrichment of prior austenite caused by the increased carbide dissolution.

The results of the M_S temperature are also shown in Fig. 5c, where it can be illustrated that the small deformation brings about no significant change in the M_S temperature while a substantial decrease in the M_S temperature occurs with a deformation degree higher than 10%, which are in a good agreement with the results of previous published one [3]. Sourmail [20] and park [21] have suggested that the increase in austenite carbon content caused by a higher austenitizing temperature would contribute to the decrease in M_S temperature. Similarly, due to the increased dissolution of carbides resulting from prior cold deformation, the increase in austenite carbon content is expected to lead to a decrease in the M_S temperature at larger deformation. Besides, it has been reported that the martensitic embryos may pre-exist at high temperature and freeze during the quenching process [22]. These pre-existing

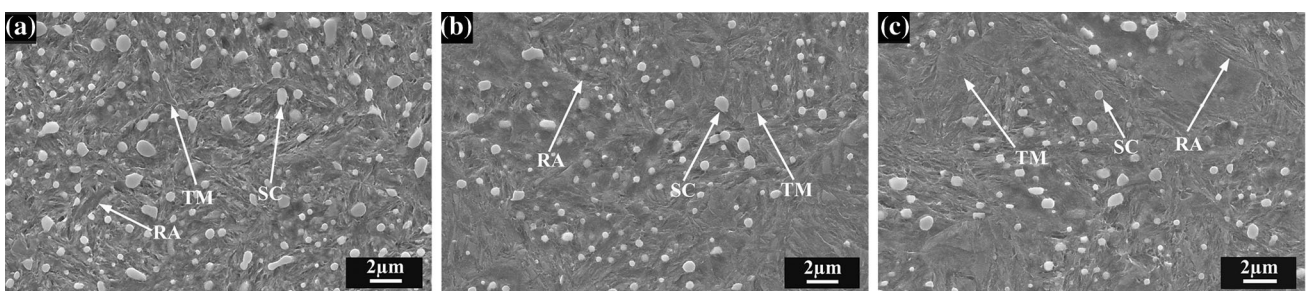


Fig. 3 Microstructures of the QT-treated specimens with different deformation degrees: a 0%; b 20%; c 50%

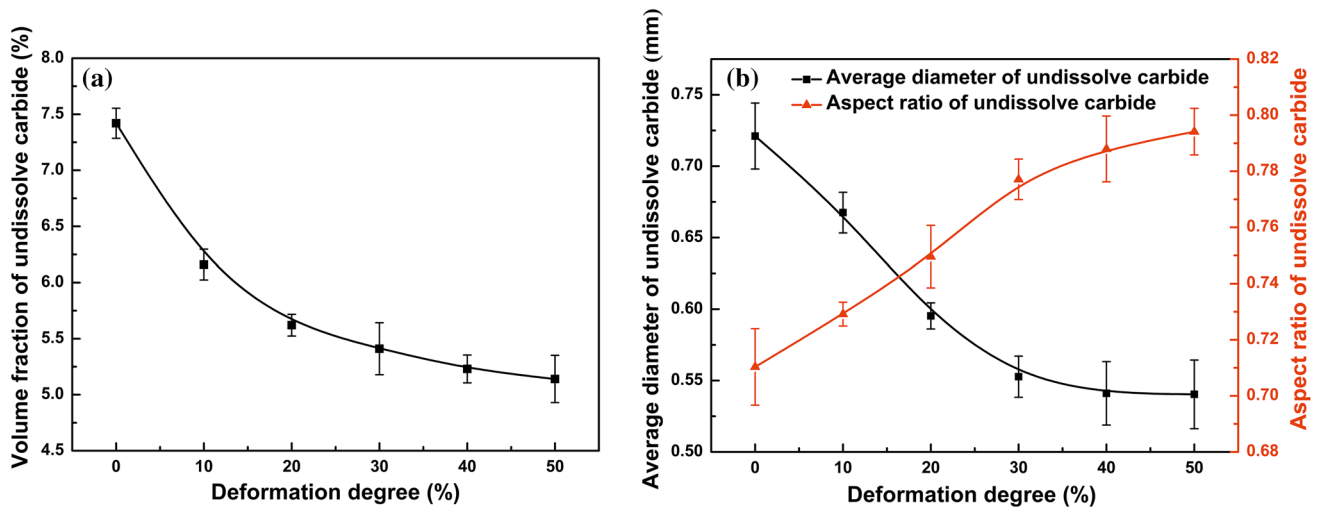


Fig. 4 a Volume fraction of undissolved carbides versus deformation degree; b average diameter and aspect ratio of undissolved carbides versus deformation degree

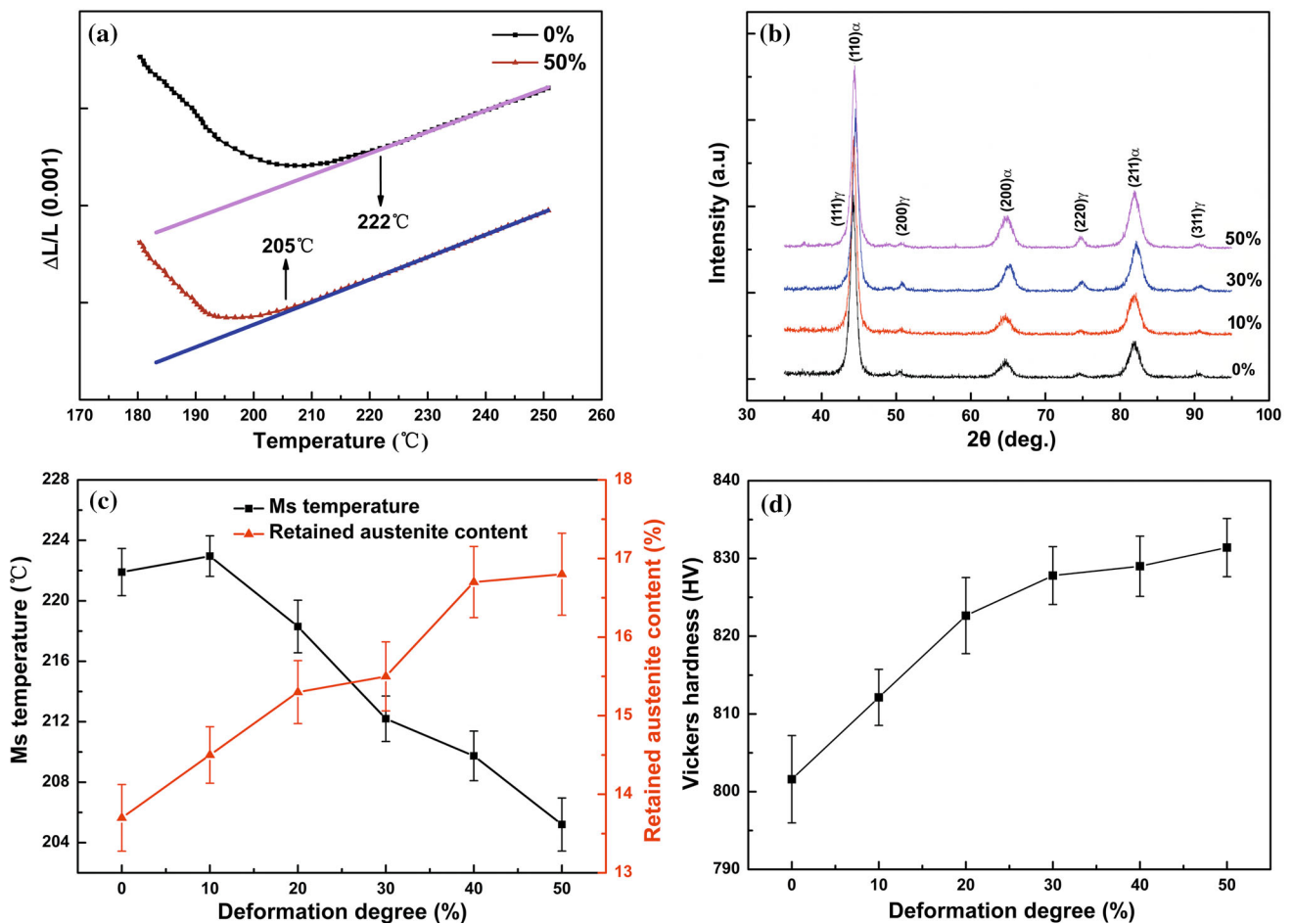


Fig. 5 a Dilatometry curves for the specimens with 0 and 50% deformation degree; b XRD spectra for the QT-treated specimens with different cold deformation degrees; c M_s temperature and the retained austenite content (after QT) versus deformation degree; d Vickers hardness of the QT-treated specimen versus deformation degree

martensitic embryos could act as a source of the local stress that triggers the martensitic transformation [23]; thus, it can be speculated that the martensitic embryos introduced by the prior cold deformation may affect the M_s temperature at small deformation. Figure 5d shows the average Vickers hardness of the QT-treated specimen increases from 802HV to 831HV with increasing deformation degree from 0 to 50%, which is associated with the refinement of prior austenite grain and the increased carbon in martensite.

Figure 6a shows the variation of carbon content in the retained austenite with different cold deformation degrees. The carbon content in retained austenite after quenching (Q) increases from 0.69 to 0.87% with the increase in deformation degree from 0 to 50%, which is consistent with the increased dissolution of carbides during the austenitization process as shown in Fig. 4. In addition, comparing the carbon content in retained austenite before and after tempering, it is found that the carbon content in retained austenite after tempering significantly increases. This increase in carbon in retained austenite verifies the partitioning of carbon from the carbon-rich martensite to austenite during the tempering process [24]. On the other hand, with the increase in deformation degree, the carbon content in retained austenite (after QT) first increases and reaches a maximum value of 1.12 at 40% cold deformation. Then, the carbon content of retained austenite decreases to 1.09 at 50% cold deformation.

In order to quantify the effect of prior cold deformation on the tempering process, the carbon partitioning behavior is evaluated by the carbon partitioning ratio (CPR), which is calculated according to $CPR = (C_{QT} - C_Q) / C_Q \times 100\%$. As shown in Fig. 6b, the value of CPR first increases and then decreases with the increase in cold deformation

degree. The results of CPR demonstrate that a moderate cold deformation (< 40%) is beneficial to the carbon partitioning, while a severe cold deformation (50%) is unfavorable for the carbon partitioning. Figure 7 shows the EBSD band contrast maps for the phase boundaries of quenched samples without deformation and with 40% deformation, indicating that the prior cold deformation leads to a higher density of phase boundaries. Consistent with the report in the literature [25], the fine austenite grains have more grain boundaries, which play a role as obstacles to the growth of the martensite and refine the fresh martensite microstructure. In addition, it is known that the boundary diffusion of elements is much faster than the volume diffusion [26]; thus, the microstructure refinement caused by the cold deformation may promote the interface diffusion of carbon atoms and would be in favor of the carbon partitioning process. On the other hand, Knijf et al. [27] have reported that the carbon flux is lower when presenting a less amount of martensite, and it will require more time to transmit the carbon from supersaturated martensite into retained austenite. Moreover, the results shown in Fig. 5c verify that the volume fraction of martensite decreases with the increase in cold deformation. In other words, there will be less martensite that acted as available carbon source for carbon partitioning, which may be unfavorable to the carbon partitioning process. Considering the two mechanisms above, one can expect that the effect of volume fraction of martensite would play the dominant role after a certain amount of deformation (40%). As a consequence, the carbon partitioning is weakened with a cold deformation higher than 40%.

As shown in Fig. 8, the TEM observation shows that the size of retained austenite accompanied with 40% cold deformation is finer compared with those without cold

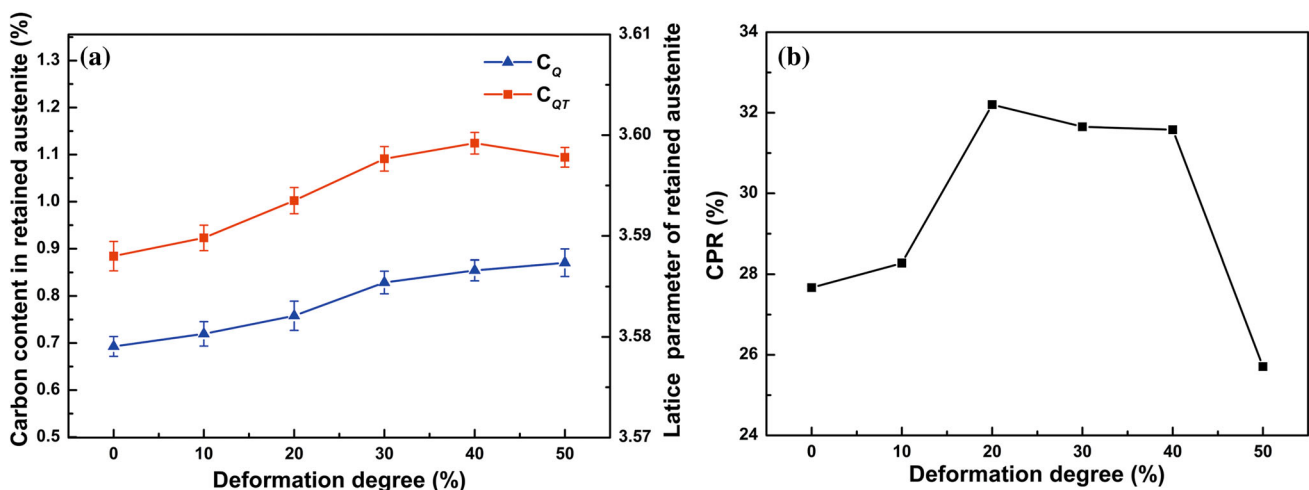


Fig. 6 **a** Carbon content in retained austenite after Q and QT versus deformation degree; **b** carbon partitioning ratio (CPR) during the tempering process versus deformation degree

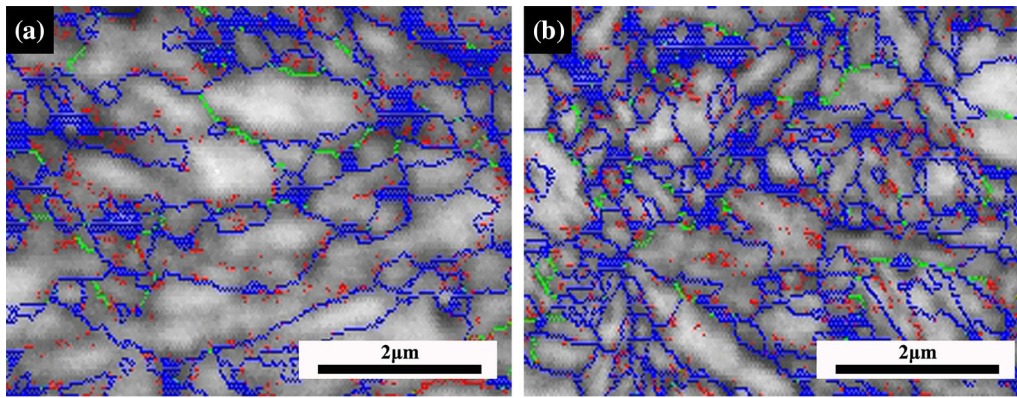


Fig. 7 EBSD band contrast maps for the phase boundaries of quenched samples: **a** without deformation, **b** with 40% deformation

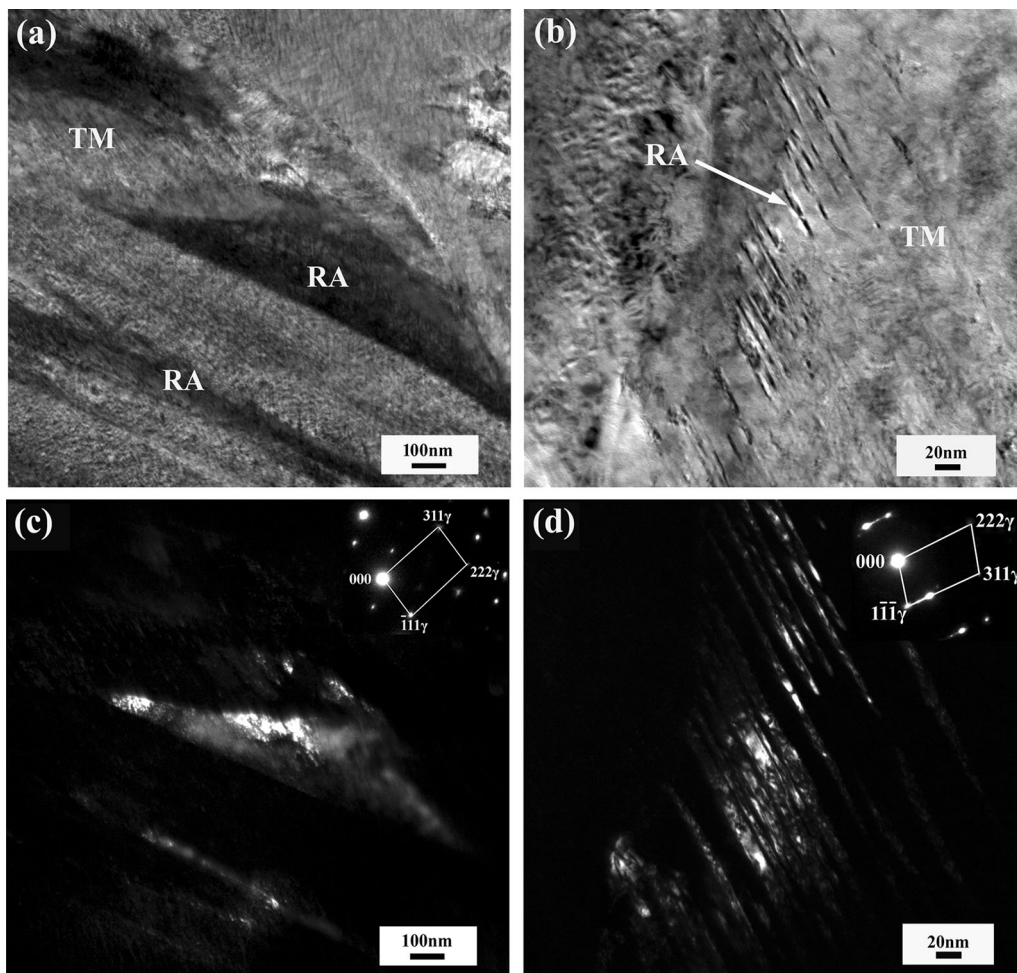


Fig. 8 TEM morphologies of retained austenite: **a, c** bright field and corresponding dark field for specimen without cold deformation; **b, d** bright field and corresponding dark field for specimen with 40% cold deformation. TM and RA represent tempered martensite and retained austenite, respectively

deformation. Meanwhile, the morphology of retained austenite changes from block to film-like. It has been reported that the isotropic transformation strain caused by the martensitic transformation can be expressed as $\varepsilon^* =$

$0.0058 + 0.0045C_\gamma$ [28]. Thus, the higher carbon content in prior austenite would increase the isotropic transformation strain due to the solid solution effect of carbon on altering the lattice parameters. As a result, the enhanced three-

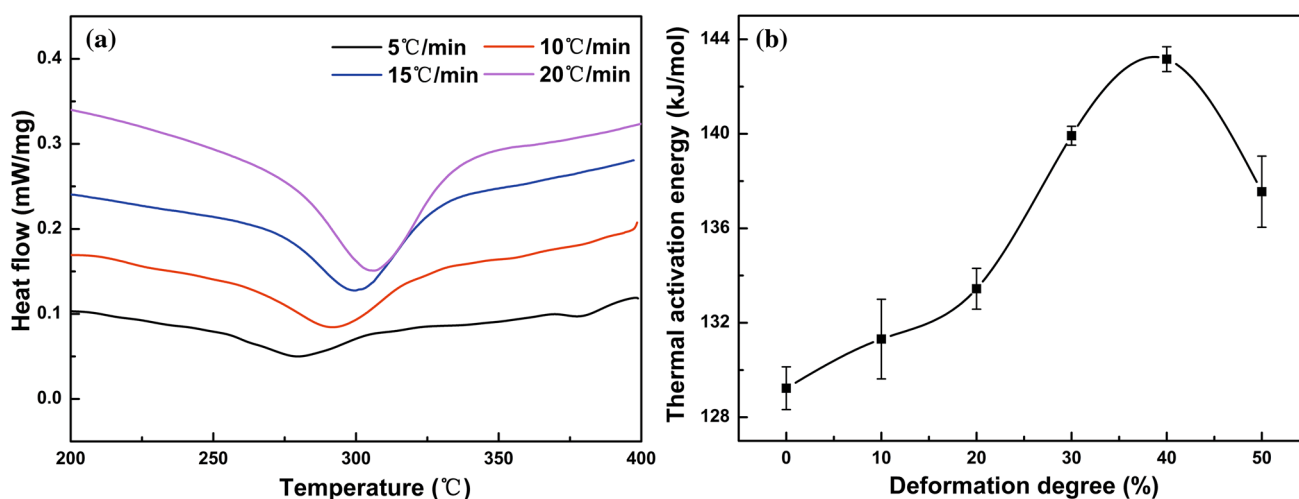


Fig. 9 **a** DSC curves of the QT-treated specimens without deformation at different heating rates of 5, 10, 15, 20 °C/min; **b** activation energy of retained austenite versus cold deformation degree

Table 2 Retained austenite contents and k values with different deformation degrees

Deformation degree (%)	Fraction of RA_0 (vol%)	Fraction of RA_e (vol%)	Compressive strain (%)	k
0	13.7	10.1	10	3.20
10	14.5	11.4	10	2.52
20	15.3	12.6	10	2.04
30	15.5	13.1	10	1.76
40	16.7	14.7	10	1.34
50	16.8	14.8	10	1.33

dimensional hydrostatic pressure would be applied on the austenite when martensitic transformation occurred, and then, the retained austenite would be finer and tends to be film-like at room temperature.

3.2 Thermal Stability of Retained Austenite

Figure 9a shows the DSC curves of the QT-treated specimens without deformation at different heating rates of 5, 10, 15 and 20 °C/min, which were used to calculate the thermal activation energy for the decomposition of retained austenite. The activation energy of retained austenite of deformed specimens was also calculated as shown in Fig. 9b. The thermal activation energy first increases from 129 kJ/mol with increasing deformation degree and reaches a maximum value of 142 kJ/mol at 40% cold deformation. Then, the thermal activation energy begins to decrease at 50% cold deformation degree. By comparing the results in Fig. 6a and Fig. 9b, it can be found that with increasing deformation degree, the variation of thermal stability is in good agreement with the trend of austenite

carbon content, which suggests that the austenite carbon content plays a super-critical role in its thermal stability.

3.3 Mechanical stability of retained austenite

The identical compressive strain (10%) was applied to the QT-treated specimens for evaluating the mechanical stability of retained austenite. Table 2 shows that the value of k decreases from 3.2 to 1.33 with the increase in the deformation degree, indicating that the mechanical stability of retained austenite is enhanced under the prior cold deformation. However, the mechanical stability is not significantly improved when the deformation degree is higher than 40%.

The research of Misra et al. [29] showed that the stacking fault energy (SFE) increased with decreasing grain size at a given temperature. Talonen [30] suggested that the mechanical transition of retained austenite became more difficult with increasing SFE. It means that more strain/stress energy will be required for strain-induced martensitic transformation in a microstructure with finer grain size. Thus, the decreasing grain size caused by prior

cold deformation will be beneficial to the mechanical stability of retained austenite. Another contributing factor to the mechanical stability of austenite is the morphology of the retained austenite. Luo [31] reported that the film-like retained austenite was surrounded by hard martensite with a higher hydrostatic pressure. Since the martensitic transformation requires volume expansion, more potential energy is necessary for the mechanical transition of retained austenite. However, Molkeri et al. [32] suggested that increasing austenite content resulted in a decrease in required activation energy for mechanical induced transformation of retained austenite. Since the results in Fig. 5c have shown that the volume fraction of retained austenite continuously increases with the prior cold deformation. It can be expected that, due to the higher volume fraction of retained austenite, the mechanical stability of retained austenite would not show a significant improvement at a larger deformation degree, whereas the contribution of grain size and morphology to the increased mechanical stability of retained austenite plays a dominant role at small deformation.

4 Conclusions

1. The prior cold deformation not only refines the prior austenite grain but also accelerates the carbide dissolution during the austenitization process, thus leading to the increased fraction and carbon content of retained austenite. It is also found that the prior cold deformation contributes to the carbon partitioning during the tempering process due to the higher density of phase boundaries. Besides, the morphology of retained austenite changes from blocky to film-like with increasing cold deformation.
2. The thermal stability of retained austenite first increases with increasing deformation degree and reaches a maximum value at 40% deformation degree. This result coincides with the trend of the carbon content in retained austenite (after QT), which is jointly determined by the carbide dissolution during austenitization and the carbon partitioning during tempering.
3. Due to the refined grain size together with the formed film-like retained austenite, the mechanical stability of retained austenite increases with the increase in deformation degree. However, the contribution to the mechanical stability would be saturated when the deformation degree is higher than 40%.

Acknowledgements The work was supported by the National Natural Science Foundation of China (Nos. 51575414 and 51605354), the 111 Project (B17034), the China Postdoctoral Science Foundation (No. 2017M612524) and the State Key Laboratory of Materials Processing and Die & Mould Technology, Huazhong University of Science and Technology (P2019-017).

References

- [1] L. Hua, J.D. Deng, D.S. Qian, J. Mater. Process. Technol. **54**, 65 (2017)
- [2] J. Beswick, Metall. Trans. A **15**, 299 (1984)
- [3] Z.X. Li, C.S. Li, J.Y. Ren, B.Z. Li, J. Zhang, Mater. Sci. Eng., A **674**, 262 (2016)
- [4] K. Rytberg, W.M. Knutson, V. Recina, Mater. Sci. Eng., A **527**, 243 (2010)
- [5] H.K.D.H. Bhadeshia, Prog. Mater. Sci. **57**, 268 (2012)
- [6] S.J. Lee, Y.K. Lee, Mater. Sci. Forum **475**, 3169 (2005)
- [7] X.H. Lu, W. Li, C.L. Wang, H.S. Zhao, X.J. Jin, Acta Metall. Sin. (Engl. Lett.) **28**, 1 (2015)
- [8] Y. Zhang, L. Wang, K.O. Findley, J.G. Speer, Metall. Mater. Trans. A **48**, 1 (2017)
- [9] E.V. Pereloma, A.A. Gazder, I.B. Timokhina, Mater. Sci. Forum **738**, 212 (2013)
- [10] E. Jimenez-Melero, R. Blondé, M.Y. Sherif, V. Honkimäki, Acta Mater. **61**, 1154 (2013)
- [11] C. Sidoroff, M. Perez, P. Dierickx, D. Girodin, *Advances in Steel Technologies for Rolling Bearings*, vol. 10 (ASTM International, Pennsylvania, 2015), p. 14
- [12] X. Qiao, L. Han, W. Zhang, J. Gu, ISIJ Int. **56**, 140 (2016)
- [13] Y.C. Liu, F. Sommer, E.J. Mittemeijer, Acta Mater. **51**, 507 (2003)
- [14] C. Wang, H. Ding, Z.Y. Tang, J. Zhang, Ironmak. Steelmak. **42**, 9 (2015)
- [15] K.I. Sugimoto, M. Kobayashi, S.I. Hashimoto, Metall. Trans. A **23**, 3085 (1992)
- [16] M. Preciado, M. Pellizzari, J. Mater. Sci. **49**, 8183 (2014)
- [17] K.I. Sugimoto, T. Iida, J. Sakaguchi, T. Kashima, ISIJ Int. **40**, 902 (2000)
- [18] G.R. Speich, A. Szirmae, Trans. TMS-AIME **245**, 1063 (1969)
- [19] J.H. Kang, P.E.J. Rivera-Díaz-Del-Castillo, Comput. Mater. Sci. **67**, 364 (2013)
- [20] T. Sourmail, V. Smanio, Acta Mater. **61**, 2639 (2013)
- [21] J. Park, J.H. Shim, S.J. Lee, Metall. Mater. Trans. A **49**, 450 (2018)
- [22] L. Kaufman, M. Cohen, Prog. Met. Phys. **7**, 165 (1958)
- [23] W. Zhang, Y.M. Jin, A.G. Khachatryan, Acta Mater. **55**, 565 (2007)
- [24] S. Matas, R.F. Hehemann, Nature **187**, 685 (1960)
- [25] C. Wang, H. Ding, Z. Tang, J. Zhang, H. Di, Steel Res. Int. **85**, 388 (2014)
- [26] M.J. Whiting, Scr. Mater. **43**, 969 (2000)
- [27] D.D. Knijf, E.P.D. Silva, C. Föjer, R. Petrov, Mater. Sci. Technol. **31**, 817 (2014)
- [28] K.I. Sugimoto, M. Misu, M. Kobayashi, H. Shirasawa, ISIJ Int. **33**, 775 (1993)
- [29] R.D.K. Misra, B.R. Kumar, M. Somani, P. Karjalainen, Scr. Mater. **59**, 79 (2008)
- [30] Appl Talonen, Surf. Sci. **123**, 339 (2007)
- [31] H. Luo, Scr. Mater. **66**, 832 (2012)
- [32] A. Molkeri, F. Pahlevani, I. Emmanuelawati, V. Sahajwalla, Mater. Lett. **163**, 209 (2016)